Effect of Different Metal Modified Dolomite Catalysts on Catalytic Glycerol Hydrogenolysis towards 1,2-Propanediol

(Kesan Mangkin Dolomit Logam Terubah Suai ke atas Tindakan Pemangkinan Hidrogenolisis Gliserol terhadap 1,2-Propanadiol)

Norsahida Azri[1,2], Ramli Irmawati[1,4,*], Usman Idris Yda-Umar[1,3], Mohd Izham Saiman[1,2] & Yun Hin Taufiq-Yap[1,2,5]

[1]Department of Chemistry, Faculty of Science, Universiti Putra Malaysia, 43400 UPM Serdang, Selangor Darul Ehsan, Malaysia

[2]Catalysis Science and Technology Research Centre (PutraCat), Faculty of Science, Universiti Putra Malaysia, 43400 UPM Serdang, Selangor Darul Ehsan, Malaysia

[3]Department of Chemical Sciences, Federal Polytechnic, PMB 55, Bida, Niger State, Nigeria

[4]Laboratory of Processing and Product Development, Institute of Plantation Studies, Universiti Putra Malaysia, 43400 UPM Serdang, Selangor Darul Ehsan, Malaysia

[5]Faculty of Science and Natural Resources, Universiti Malaysia Sabah, 88400 Kota Kinabalu, Sabah, Malaysia

ABSTRACT

A series of metal modified dolomite catalysts (10%Ni-20%Cu/Dol, 10%Co-20%Cu/Dol, 10%Fe-20%Cu/Dol, 10%Zn-20%Cu/DolNi) were synthesized via method of impregnation, later calcined at 500 °C and reduced by 5%H_2 at 600 °C. Those catalysts were formerly tested for their physico-chemical properties by BET, BJH, XRD, H_2-TPR, NH_3–TPD, CO_2-TPD and SEM, and followed by evaluation in catalytic performance of glycerol hydrogenolysis to 1,2-propanediol (1,2-PDO). Among the examined catalysts, 10%Ni-20%Cu/Dol showed optimum hydrogenolysis activity owing to the good copper-nickel-dolomite interaction. The outcomes from the characterizations disclosed that the presence of nickel-copper species which principally enriched on dolomite surface thereby enhanced the properties of the catalyst in terms of good metal reducibility along with the presence of adequate catalyst acidity. All the good features of 10%Ni-20%Cu/Dol catalyst added to its high activity with 83.5% glycerol conversion (GC) and 75% 1,2-PDO with low methanol as side reaction product under 200 °C, 4 MPa H_2 and 10 h duration test, 1 g catalyst dosage and 20 wt% glycerol concentration.

Keywords: Acidity; dolomite; hydrogenolysis; modified catalyst; 1,2-propanediol

ABSTRAK

Satu siri mangkin terubah suai dolomit (10%Ni-20%Cu/Dol, 10%Co-20%Cu/Dol, 10%Fe-20%Cu/Dol, 10%Zn-20%Cu/DolNi) telah disintesis menggunakan kaedah pemadatan lalu dikalsinkan pada 500 °C dan diturunkan ke 5%H_2 pada 600 °C. Sifat fiziko-kimia mangkin telah dikaji dengan menggunakan pelbagai kaedah analisis termasuk BET, BJH, XRD, H_2-TPR, NH_3-TPD, CO_2-TPD dan SEM dan kemudian diuji dalam hidrogenolisis gliserol terhadap 1,2-propanadiol dalam tindak balas akues. Antara mangkin yang diuji, 10%Ni-20%Cu/Dol menunjukkan hasil hidrogenolisis yang optimum, yang didorong oleh interaksi baik antara nikel-kuprum-dolomit. Hasil pencirian mangkin menunjukkan bahawa kehadiran nikel-kuprum spesies pada permukaan dolomit dan ini membantu sifat mangkinan seperti penurunan logam yang baik dan kehadiran kapasiti asid mangkin yang sesuai. Kesemua sifat mangkin 10%Ni-20%Cu/Dol telah membantu dalam kecemerlangan pemangkinan dengan penurunan gliserol dan pemilihan terhadap 1,2-PDO yang terbaik dengan masing-masing 83.5 and 75% pada suhu tindak balas 200 °C, tekanan hidrogen 4 MPa, masa tindak balas 10 jam, kepekatan gliserol 20 bt% dan berat mangkin 1 g.

Kata kunci: Asiditi; dolomit; hidrogenolisis; mangkin terubah suai; 1,2-propanadiol

INTRODUCTION

It has been known that 1,2-propanediol (1,2-PDO) was used as a chemical additive in the manufacture of mainly pharmaceuticals, cosmetics, solvent in food, and as raw material for polyester resins (Gallegos-Suarez et al. 2015). The estimated global production of 1,2-PDO reached about 1.4 million tons yearly (Vasiliadou & Lemonidou 2011). Conventionally, its manufactured was via chlorination and hydration reaction process using propylene oxide derived petroleum (Bagheri et al. 2015; Rajkhowa et al. 2017). The concern of dwindling wealth of petroleum in addition to the environmental pollution topic, therefore, the production of 1,2-PDO from renewable bases could be necessitated as it could also substantively alter the market cost of 1,2-PDO. Meanwhile the excess of glycerol from biodiesel production could serve as an ideal material for the production of 1,2-PDO (Pandhare et al. 2016). Hydrogenolysis of glycerol to 1,2-PDO involves C=O bond activation on acid sites and hydrogenation of dehydrated intermediate product to form 1,2-PDO on metal sites (Balaraju et al. 2009; Gandarias et al. 2012; Mallesham et al. 2016; Zheng et al. 2015) (Scheme 1).

Considerable efforts have been dedicated to glycerol hydrogenolysis using heterogeneous catalysts such as Ru and Ce and transition metal-based catalysts such as Cr, Co, Ni, Cu, Zn and Zr (Soares et al. 2016a; Xia et al. 2011; Yu et al. 2010). However, for a cost effective catalyst application, the use of economical metal-based catalysts are more look up since they also exhibited high in catalytic activity. Cu-based catalysts have been said to perform well in catalytic performance attributable to its efficiency towards C=O bond cleavage (C=O bond activation) rather than C-C bond cleavage (Freitas et al. 2018; Putrakumar et al. 2015). Further, a modification of Cu based-catalyst with co-catalysts or promoters (Ni, Co and Fe) have also been reported to improve and strengthen the interaction between the metals as high 1,2-PDO selectivity and glycerol conversion of > 60% over metal modified catalysts was attained (Gandarias et al. 2012; Jiang et al. 2016; Pudi et al. 2015; Soares et al. 2016b). The catalytic efficiency made known by metal modified catalyst was owing to the synergetic metals interaction which for that reason enhanced the crystallite size, metallic dispersion, acidity and metal reducibility of the catalyst (Jiang et al. 2016; Pandhare et al. 2016; Pudi et al. 2015; Soares et al. 2016a).

For this work, dolomite with low-priced, highly abundance in Perlis, Malaysia and high acidic characteristic with mainly derived from calcium carbonate ($CaCO_3$) and magnesium carbonate ($MgCO_3$) has been selected as a catalyst support for the metal catalysts. The performance of the metal modified dolomite catalysts was then tested in glycerol hydrogenolysis to 1,2-PDO under 200 °C, 10 h and 4 MPa H_2 to relate the role of catalyst metal reducibility and catalyst acid capacity in the reaction performance. Meanwhile, impregnation method was preferred for catalyst preparation as it may control the catalyst metal size rather than by co-precipitation method (Azri et al. 2020). This could be attributed to during wet impregnation, an excess of solution containing the precursor of solid phase is used. The solid is then dried and the excess solvent is removed. It is the procedure whereby the maximum solubility of the precursor in the solution is limited. This method offers easy way to prepare a layer of active matter on the catalyst surface. This could be attributed to the solution transport from a capillary action process to a diffusion process, which is much slower. This feature made impregnation method as an effective process for the production of catalyst.
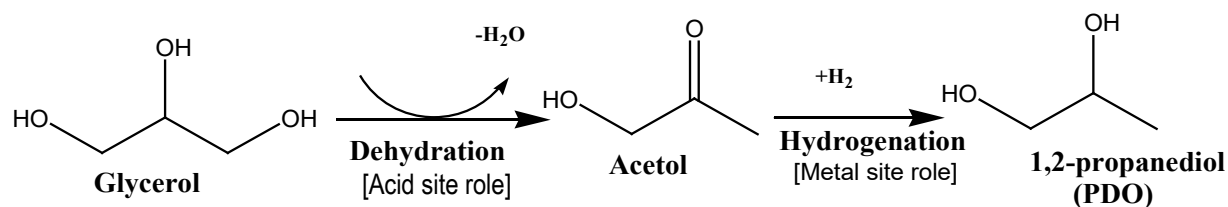
SCHEME 1. Glycerol hydrogenolysis reaction pathway in acidic condition
(Mallesham et al. 2016)

MATERIALS AND METHODS

Dolomite was obtained from Perlis Dolomite Industries, Malaysia while copper precursor derived nitrate hexahydrate ($Cu(NO_3)_2.6H_2O$) ($\geq$ 99%), nickel precursor derived nitrate hexahydrate ($Ni(NO_3)_2.6H_2O$) ($\geq$ 99%) and cobalt precursor derived nitrate hexahydrate ($Co(NO_3)_2.6H_2O$) ($\geq$ 99%) were all supplied by R&M Chemical Company, Malaysia. Both iron

precursor derived nitrate nanohydrate ($Fe(NO_3)_3.9H_2O$) (99%) and zinc precursor derived nitrate hexahydrate ($Zn(NO_3)_2.6H_2O$) (98%) were purchased from Bendosen Company. The main feedstock glycerol ($\geq$ 99.5%) was from Sigma-Aldrich.

The metal modified dolomite catalysts were all prepared via impregnation method. Prior for catalyst preparation, nickel loading was fixed at 10 wt% while copper loading was at 20 wt%. The usual synthesis required 2.4 g of nickel nitrate hexahydrate and 3.8 g of copper nitrate hexahydrate which were then separately dissolved in 10 mL distilled water and was then poured into a 4 g dolomite powder, stirred at 300 rpm and oven dry at 90 °C for 3 h. The resultant mixture was then completely dry in oven at 120 °C for 24 h, later on calcined at 500 °C for 3 h in a furnace under static air (10 °C/min) and reduced by 5% H_2/Ar (2 °C/min) at 600 °C for 3 h. The synthesized catalyst was denoted as 10%Ni-20%Cu/Dol. The other metal modified catalysts namely 10%Co-20%Cu/Dol, 10%Fe-20%Cu/Dol and 10%Zn-20%Cu/Dol were all prepared using similar preparation method as indicated above.

CATALYST CHARACTERISATION

All characterization procedures used in this study with the exception of CO_2-TPD were similar with the one reported in our previously published paper. As for CO_2-TPD, the catalyst sample was carried out using temperature programmed desorption and carbon dioxide was used as probe gas (CO_2-TPD) (Thermo-Finnigan TPD/R/O 1100 SERIES). Prior to analysis, the sensitivity of TCD signal was calibrated using CuO powder by pulse chemisorption (Karelovic & Ruiz 2015) technique. Next, the test was carried out using ~0.05 g of catalyst sample into a U-tube TPD quartz and was then saturated under CO_2 flow at 30 mL/min for 1 h. Lastly, the desorption analysis of the treated CO_2 catalyst was carried out by heating the sample under helium flow (30 cm³/min) from 50 to 1000 °C at a rate of 10 °C/min. The corresponding amount of basic sites was assessed by integrating the desorption peak obtained from the analysis.

REACTION TEST

The reaction set up for hydrogenolysis in this study was similar and detailed in our previous report (Karelovic & Ruiz 2015). The catalytic tests were conducted in a 150 mL stainless steel autoclave reactor (SS316L series) equipped with Teflon lining cup, an electrical heating jacket and a magnetic stirrer. In a typical experiment, the autoclave reactor was charged with 4 g glycerol solution, 16 g distilled water, and 1 g synthesized catalyst. The reactor then was purged and pressurized with H_2 to the desired pressure. Afterwards, the reactor was heated in a defined reaction time for hydrogenolysis reaction. During the catalytic reaction, the reactor was set at maximum H_2 pressure, temperature and time of 4 MPa, 200 °C and 10 h, respectively. For all catalytic reactions, the reactor was left stirred at 400 rpm. The reaction starting time was defined once the reactor temperature reached the desired reaction temperature. After completion of the reaction, the reactor was cooled down to room temperature, and the obtained liquid product was collected and separated from the catalyst by centrifugation process at 3000 rpm for 15 min. For comparison study, a blank reaction (reaction being conducted without the presence of any catalyst powder and/or support) was also performed at similar reaction parameters.

PRODUCT ANALYSIS

The procedure step for product analysis in this study was similar to our previous report (Karelovic & Ruiz 2015). The obtained liquid product from glycerol hydrogenolysis reaction was analyzed using gas chromatography-flame ionization detector (GC-FID) equipped with HP-5 capillary column (length: 30 m × inner diameter: 0.32 mm × film thickness: 0.25 µm). It was operated at 300 °C with splitless inlet mode. Prior to analysis, the liquid product was extracted using ethyl acetate in a 1:1 ratio. The extraction was carried out three times. Subsequently, the product solution was dried in oven at 70 °C for 15 min in order to concentrate the solution. Lastly, a derivatization process was charged to the liquid sample before it is being analyzed by GC analysis. Typically, N-O-bis(trimethylsilyl) trifluroacetamide (BSTFA) was used as the silyl agent and was mixed with pyridine (C_5H_5N) as binding solvent in a 1:1 ratio and was then left dried in oven for 20 min at 60 - 70 °C so as to achieve complete silylation process. 1 µL amount of the derivatized product was directly injected to GC. The initial temperature was determined at 40 °C and held for 6 min with rate of 7 °C min⁻¹ towards reaching the final temperature of 270 °C. The temperature for injection was set at 250 °C. The glycerol conversion and the selectivity of product were acquired by comparing the retention time of standard with the obtained experimental-based products on GC chromatogram peak. The equations for calculation of

glycerol conversion and 1,2-PDO selectivity are depicted in (1) and (2), respectively.

$$\text{Glycerol conversion, } \% = \frac{C_{glycerol_{in}} - C_{glycerol_{out}}}{\sum C_{glycerol,in}} \times 100\% \quad (1)$$

where $C_{glycerol'in}$ is described as the initial concentration of glycerol and $C_{glycerol'out}$ as the final concentration of glycerol. And C_{total} is the sum of the product detected in the liquid product. (All peaks regarded to the product in this study were confirmed by the peak of standard solution).

RESULTS AND DISCUSSION

N$_2$-PHYSISORPTION ANALYSIS

As indicated in Table 1, BET surface area of all the metal modified catalysts dropped when compared to dolomite (13.3 m^{2}g^{-1}) ranks as dolomite > 10%Co-20%Cu/Dol > 10%Ni-20Cu%/Dol > 10%Zn-20%Cu/Dol > 10%Fe-20%Cu/Dol. This attributable to the filling of the support pores by the metal species in line with the report of Thirupathi and Smirniotis (2012) indicated that the decrease in surface area of Mn–Ni(0.4)/TiO$_2$ was caused by the loaded nickel oxide in catalyst support. At the same time, pore volume was also reduced along with decrease in surface area from 0.276 (dolomite) to 0.083 cm^{3}g^{-1}. This attributable to the covered catalyst pores or blocked pores structure by metal species as also reported by Zhao et al. (2013).

TABLE 1. Physicochemical properties of the catalysts

Catalyst	BET	XRD			H$_2$-TPR		Total amount H$_2$ consumed[d] (μmol/g)	NH$_3$-TPD	CO$_2$-TPD
	Surface area[a] (m^{2}g^{-1})	Pore volume[b] (cm^{3}g^{-1})	Pore diameter[b] (Å)	Crystallite size (nm)[c]	H$_2$ consumed at different temp[d] (μmol/g)			Total amount NH$_3$ adsorbed[e] (μmol/g)	Total amount CO$_2$ adsorbed[f] (μmol/g)
					150-550 °C	> 550 °C			
Dolomite	13.3	0.276	152.02	27.4	-	1005	1005	16149	451
10%Ni-20%Cu/Dol	5.2	0.099	24.33	48.3	28308, 5262	10853, 9545	53968	10184	1101
10%Co-20%Cu/Dol	6.8	0.091	24.33	41.4	41482, 14637	13873	69992	29574	1502
10%Fe-20%Cu/Dol	4.4	0.083	86.63	29.0	34660, 5635,	3625, 27228	71148	14635	795
10%Zn-20%Cu/Dol	4.8	0.148	24.22	96.4	29355, 6002	12422	47779	12499	972

[a]Determined using BET method, [b]Determined using BJH method, [c]The data were estimated according to the Debye Scherrer equation using the FWHM of the dolomite peak at 2θ = 62.4°, [d]H$_2$-TPR peak for all catalysts, [e]NH$_3$-TPD desorption peak for all catalysts, and [f]CO$_2$-TPD desorption peak for all catalysts

Also, the decrease in catalyst surface area was supported by the decrease in catalyst pore volume as it dropped from 156.34 Å (dolomite) to 19.07 Å. It was noted that both 10%Ni-20%Cu/Dol and 10%Co-20%Cu/Dol catalysts presented smaller in both pore diameter and pore volume. This however much likely be associated to the formation of new pores as reaction sites on the catalyst surface. This was advantage as it could prevent the metal active sites from being easily leached during catalytic reaction rather lead to the tougher interaction of reaction sites during reaction performance.

Meanwhile, catalysts isotherms in Figure 1(A) and 1(B) are all catalysts fall under the type III classification, indicating the typically macroporous solid materials of weak adsorption-desorption interaction between adsorbed and the desorbed molecules in line with IUPAC classification. The observed hysteresis p/p° > 0.8 in

Figure 1(B) disclosed the typical aggregates of plate-like particles with non-rigid particles size (Luna et al. 2018). Moreover, all catalysts exhibited lower amount of N_2 adsorbed (~ 1 cm^3g^{-1}) derived from the characteristic of clustered solid catalyst while the pore size distributions of all catalysts were under values of 2 to 50 nm.
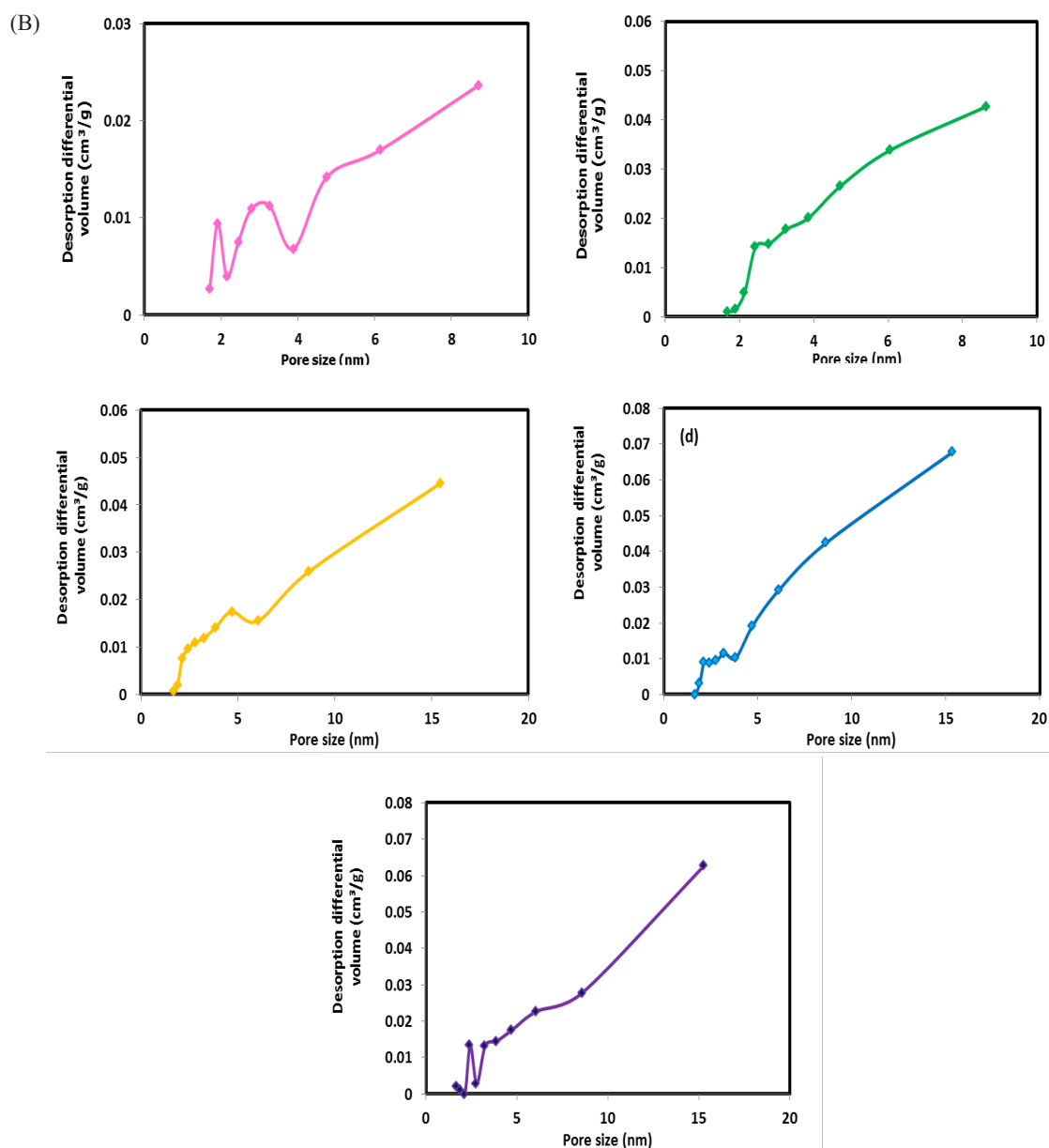
(B)
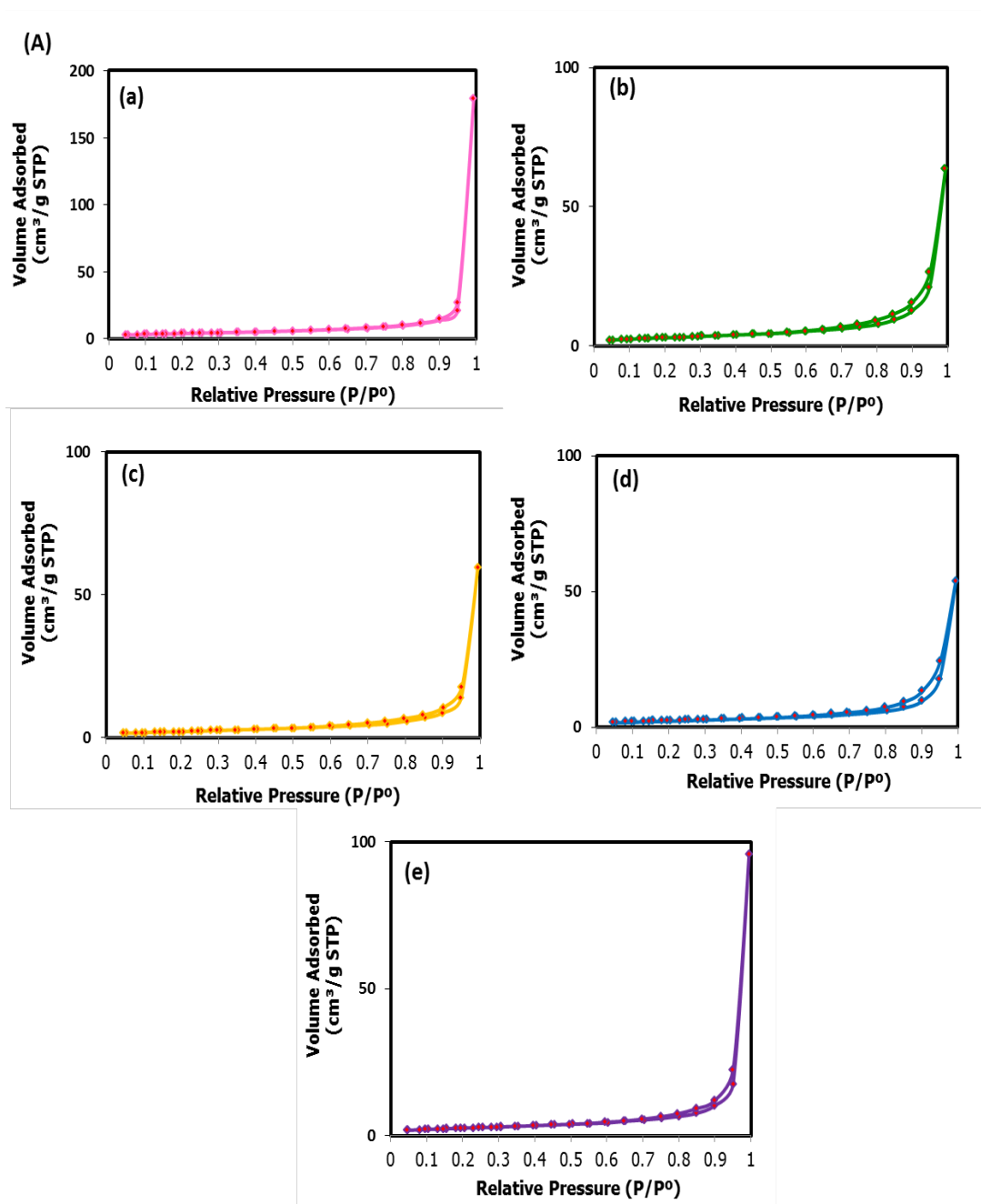
FIGURE 1. N$_2$ adsorption-desorption isotherms (A) and pore size distribution (B) of (a) dolomite, (b) 10%Ni-20%Cu/Dol, (c) 10%Co-20%Cu/Dol, (d) 10%Fe-20%Cu/Dol and (e) 10%Zn-20%Cu/Dol

X-RAY DIFFRACTION (XRD)

XRD patterns of dolomite in Figure 2(A) exhibit mixed crystalline phases of CaMg$_2$ at 2θ =18.1º, 28.3º and 33.8º (JCPDS; 01-1070), dolomite phase (JCPDS; 02-0767) at 2θ = 37.51º, 50.76º, and 62.20º, MgCO$_3$ phase (JCPDS; 02-0871) at 2θ = 44.2º and 47.4º, CaO phase at 2θ = 32.4º and 54.2º (JCPDS; 01-1160) and MgAl$_2$O$_4$ phase at 2θ =

78.7º (JCPDS; 03-1160). Most of the phases presented rather lower in intensity than dolomite as a result of the embedment of metal oxides in the dolomite matrix. As well, metal oxide phases such as CuO at 2θ = 35.5º and 38.8º (JCPDS; 44-0706), NiO at 2θ = 37.2º (JCPDS; 01-1239), Co$_2$O$_3$ at 2θ = 31.1º (JCPDS; 02-0770), Fe$_2$O$_3$ at 2θ = 49.1º and 59º (JCPDS; 02-0915) and ZnO at 2θ = 36.8º and 57.3° (JCPDS; 03-0888) were also seen.
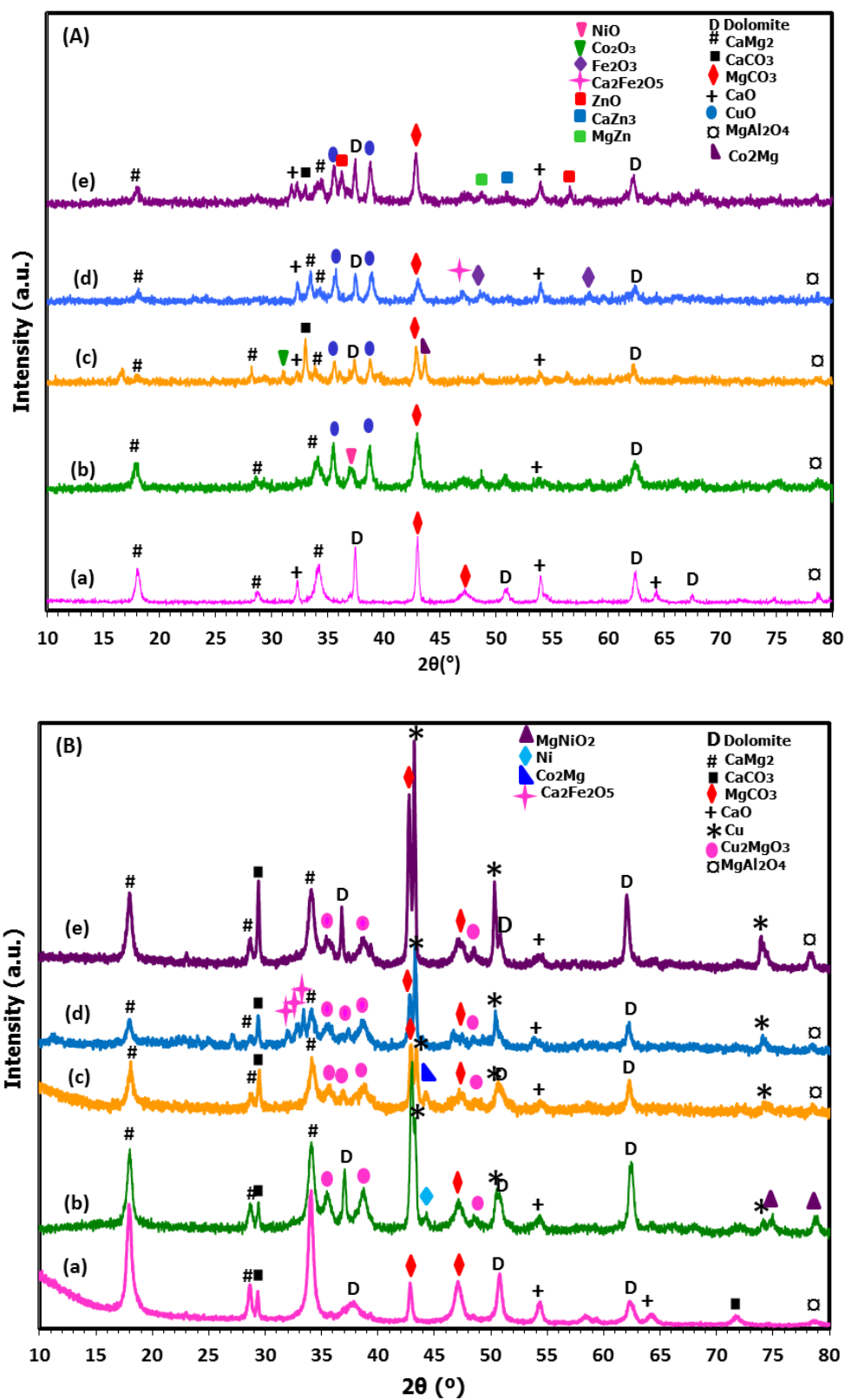
FIGURE 2. XRD diffractograms of calcined (A) and reduced samples (B) of (a)
dolomite, (b) 10%Ni-20%Cu/Dol, (c) 10%Co-20%Cu/Dol, (d) 10%Fe-20%Cu/Dol and
(e) 10%Zn-20%Cu/Dol

Meanwhile, an alloy phases of Co_2Mg at $2\theta = 44.7°$ (JCPDS; 29-0486), $Ca_2Fe_2O_5$ spinel at $2\theta = 47.8°$ (JCPDS; 02-0936), MgZn at $2\theta = 49.5°$ (JCPDS; 08-0206) and $CaZn_3$ at $2\theta = 51.3°$ (JCPDS; 35-1159) were also spotted. This was similar to previous studies which stated that the formation of spinel was more likely to be formed for metal oxide species supported on limestone solid containing Mg and Ca (Kovanda et al. 2001; Pardeshi & Pawar 2010). Markedly, none metallic peak was seen in all calcined samples.

In Figure 2(B), new peaks seen such as $CaCO_3$ at $2\theta = 29.3°$ and $72.2°$ (JCPDS; 01-1032) in reduced dolomite apart from the peaks previously detected in calcined dolomite. Notably, the CuO ($2\theta = 35.5°$ and $38.8°$) and NiO peaks ($2\theta = 37.2°$) were disappeared instead the metallic Cu ($2\theta = 43.5°$, $50.3°$ and $74.1°$) (JCPDS; 085-1326) and metallic Ni peaks ($2\theta = 44.3°$) (JCPDS; 001-1260) were appeared. The mentioned peaks were also reported by Vargas-Hernández et al. (2014) and Wen et al. (2013). Those with oxide peaks of Cu_2O and Ni_2O was not detected in 10%Ni-20%Cu/Dol catalyst, showing that the oxide species reduction by H_2 at 600 °C was complete (Gandarias et al. 2012; Zhao et al. 2013; Zhu et al. 2013).

The reduction of reducible oxides on dolomite happened through migration of electron via redox reaction on catalyst surface (Nagaraja et al. 2007). It was suggested that the presence of CaO, $CaMg(CO_3)_2$ and $MgCO_3$ species could involve in the reduction for copper and nickel oxide as calcium and magnesium was known as an agent for reduction (Tasyurek et al. 2008). Besides, spinel species were also found such as Cu_2MgO_3 ($2\theta = 35.3°$, $37.5°$, $38.2°$ and $48°$) and $MgNiO_2$ ($2\theta = 75.3°$ and $79.2°$).

It was also noted that there were no metallic species of Co, Fe, and Zn was observed in 10%Co-20%Cu/Dol, 10%Fe-20%Cu/Dol and 10%Zn-20%Cu/Dol catalysts rather their Co_2Mg ($2\theta = 44.1°$) and $Ca_2Fe_2O_5$ ($2\theta = 32°$, $33°$ and $34°$) phases were detected suggesting that upper reduction temperature is needed for their metallic formation. In all metal modified catalysts, the intensity of $MgCO_3$ phase at $2\theta = 43.5°$ was showed higher due to the growth of crystallite upon incorporation of metals into dolomite matrix.

From Table 1, the crystallite size lines as 10%Zn-20%Cu/Dol > 10%Ni-20%Cu/Dol > 10%Co-20%Cu/Dol > 10%Fe-20%Cu/Dol > dolomite. The orientated crystallite size was attributable to the behaviour of metal species occupying the interstitial dolomite bulk, therefore increased the catalyst crystal size. This could

be connected to the non-shifted peak of $MgCO_3$ phase at $2\theta = 43.5°$ and $47.4°$, with respect to dolomite support which presumably suggesting that the metal promoter was incorporated with support (Asikin-Mijan et al. 2018). In conclusion, the presence of CuO, NiO, Co_2O_3, Fe_2O_3, and ZnO on dolomite surface for respective modified catalysts in this study showed the successful impregnation of those metal species on catalyst surface.

TEMPERATURE-PROGRAMMED REDUCTION OF HYDROGEN (H_2-TPR)

From Figure 3, all metal modified dolomite catalysts exhibited with lower reduction peaks at 264-308, 418-455, and 596-630 °C as opposed to dolomite support (639 °C). Further, the peak of all modified catalysts emerged to be broader and higher than dolomite. This attributable to the alloy species reduction which thereby consumed more hydrogen and later enlarged the peak (Li et al. 2009). Previous study indicated that the broader reduction peak was initiated by the interphase hydrogen adsorption (slow adsorption) of metal alloys in their work when Cu was loaded to Ru/ZrO_2 (Soares et al. 2016b).

In this study, the reduction peak at 264-308 °C were associated to the copper oxide reduction from bulk which had insufficient interaction with dolomite to metallic Cu as it was previously reported that the non-associated CuO species was reduced to metallic Cu at < 300 °C. Meanwhile peak at 418-455 °C was credited to the reduction of CuO in interstitial dolomite since Cu-containing mixed oxide such as copper involved in aluminate spinel ($CuAl_2O_4$) and complex copper of $Cu_xMg_xAl_2O_4$ was reduced at higher temperature of 400-750 °C (Tanasoi et al. 2009; Vargas-Hernández et al. 2014; Wen et al. 2013; Zhu et al. 2013). This highly corroborated with the copper oxide reduction in dolomite crystallite as Cu_2MgO_3 peak could be detected in XRD spectrum. Generally, during reduction, Cu^{2+} ions were transformed to Cu^+ ions ($CuO \rightarrow Cu_2O$) and later reduced to metallic copper ($Cu_2O \rightarrow Cu^0$). For peak at 596 - 630 °C, it was credited to dolomite reduction as it was close to the peak maximum of bulk dolomite (639 °C).

Particularly, in the case of 10%Ni-20%Cu/Dol and 10%Fe-20%Cu/Dol catalysts, additional reduction peaks were detected at higher temperature of 957 °C and 791 °C, respectively, suggesting that the reduction of nickel and iron oxide species with dolomite in the form $MgNiO_2$ and $Ca_2Fe_2O_5$ spinel took place. As also stated by Srivastava et al. (2017) higher reduction profile of

Ni/Al$_2$O$_3$ catalyst was attributed to the reduction of NiO that strongly contacted with Al$_2$O$_3$ or also due to alloy reduction of NiAl$_2$O$_4$. Notably, 10%Ni-20%Cu/Dol might predominantly be reduced than other catalysts in line with its lowest reduction temperature at 264 °C. The presence of metallic Cu and Ni species in XRD peak may connected with its high reducibility character.
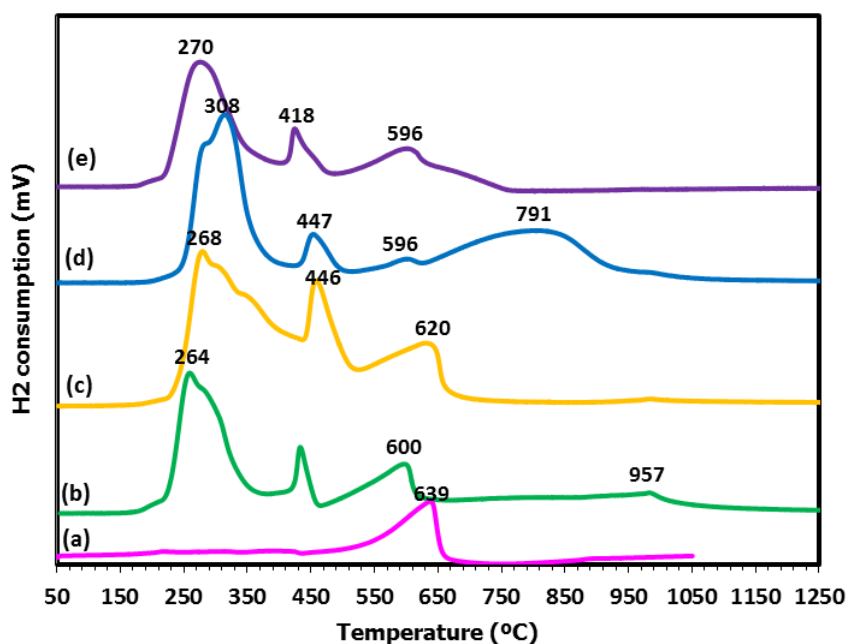

FIGURE 3. H$_2$-TPR profiles of (a) dolomite, (b) 10%Ni-20%Cu/Dol, (c) 10%Co-20%Cu/Dol, (d) 10%Fe-20%Cu/Dol and (e) 10%Zn-20%Cu/Dol

From Table 1, the total hydrogen consumption ranks as 10%Fe-20%Cu/Dol > 10%Co-20%Cu/Dol > 10%Ni-20%Cu/Dol > dolomite > 10%Zn-20%Cu/Dol. The high amount of H$_2$ consumed for metal modified catalysts with the exclusion of 10%Zn-20%Cu/Dol suggesting that some support species could be directly involve during the reduction reaction, as also suggested by Zhao et al. (2019). For that reason, the consumed hydrogen of reducible oxide species was enhanced over higher surface contact area. The CaCO$_3$, MgCO$_3$, CaO and MgAl$_2$O$_4$ phases could also be considered for the hydrogen consumption as well as metal reduction.

TEMPERATURE-PROGRAMMED DESORPTION OF AMMONIA (NH$_3$-TPD)

It is known that the presence of surface acid sites would propagate the activation of glycerol C=O bond via dehydration step (Zhu et al. 2013). Thus, the determination of acid sites of all catalysts was performed by NH$_3$-TPD analysis and the results as presented in Figure 4 and Table 1. The high desorption peaks of all catalysts above 500 °C indicated that the presence of stronger catalyst acidity. For dolomite, two peaks at 805 °C and a shoulder at 874 °C were appeared. Noticeably, desorption profile of all metal modified catalysts was shifted towards lower temperature than dolomite from 805-874 °C (dolomite) to 700-786 °C (modified catalyst). In the meantime, the second desorption peak seemed to be positioned higher than that of dolomite. Among the catalysts, 10%Co-20%Cu/Dol performed with the higher and broader desorption peak (at 772 °C) than other catalysts as a result of good interaction between cobalt-copper-dolomite species.

The acidity data from Table 1 showed that when metal promoters loaded to dolomite, different acid amount was generated which ranks as 10%Co-20%Cu/Dol > dolomite > 10%Fe-20%Cu/Dol > 10%Zn-20%Cu/Dol > 10%Ni-20%Cu/Dol. Acidity of dolomite was reduced from 16149 µmol/g to 10184, 14635, 12499 µmol/g for nickel-copper, iron-copper and zinc-copper
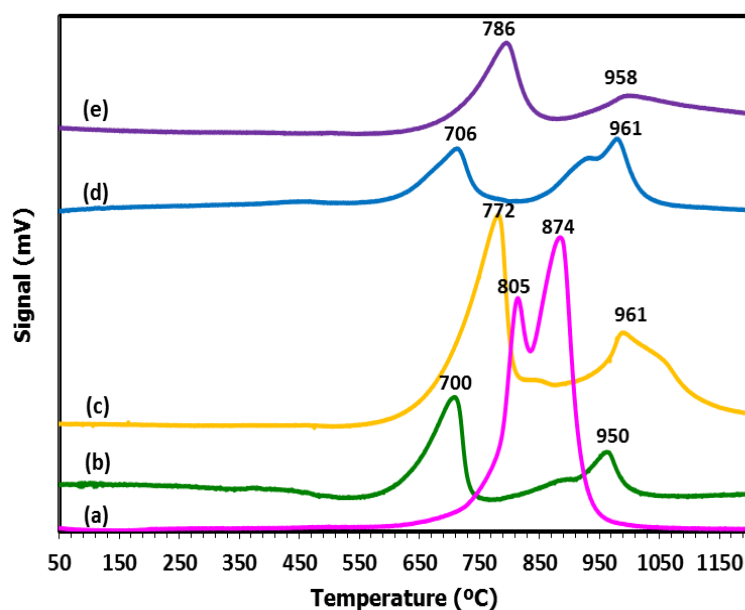
FIGURE 4. NH$_3$-TPD profiles of (a) dolomite, (b) 20%Cu/Dol, (c) 10%Ni-20%Cu/ Dol, (d) 10%Co-20%Cu/Dol, (e) 10%Fe-20%Cu/Dol and (f) 10%Zn-20%Cu/Dol

catalyst, respectively. This might evidence the metal species coverage on dolomite surface, therefore limit the NH$_3$ gas accessibility to catalyst pore which also agreed with the work of Priya et al. (2017) using metal-promoted mordenite catalyst. The acidity of dolomite containing catalysts was associated with the carbonate-rich species such as MgCO$_3$ and CaCO$_3$ phases which involve in chemisorption of NH$_3$ gas.

TEMPERATURE-PROGRAMMED DESORPTION OF CARBON DIOXIDE (CO$_2$-TPD)

In addition to acidity study, CO$_2$-TPD analysis was also performed to investigate the basic sites distribution of all catalysts. The profile of CO$_2$ adsorption and the resultant basicity data are illustrated in Figure 5 and Table 1, respectively. The strength of CO$_2$ desorption peak derived temperature was denoted as low (250
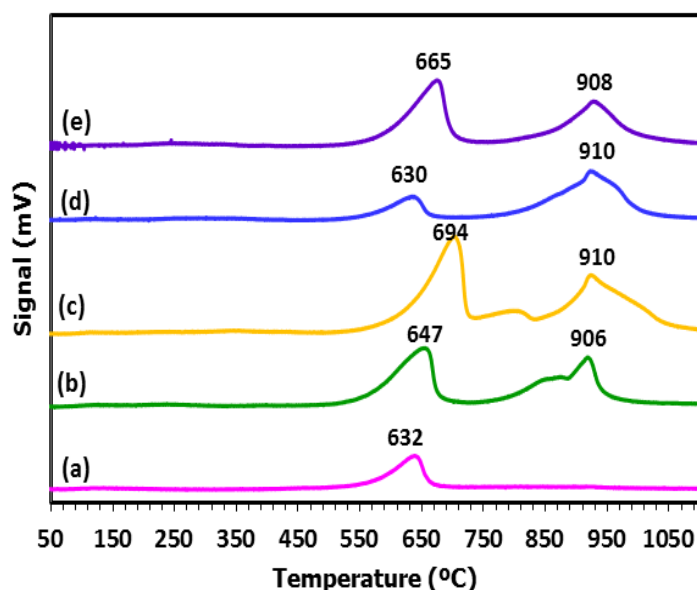
FIGURE 5. CO$_2$-TPD profiles of (a) dolomite, (b) 10%Ni-20%Cu/Dol, (c) 10%Co-20%Cu/Dol, (d) 10%Fe-20%Cu/Dol and (e) 10%Zn-20%Cu/Dol

°C), moderate (250 - 500 °C), and strong (> 500 °C) (Rahman et al. 2019). From Figure 5, all catalysts exhibited strong basicity with desorption peak at > 500 °C. Particularly, for metal modified catalysts, the second desorption peak was detected at higher temperature of ~ 900 °C indicating more basic sites on the catalyst surface. From Table 1, catalyst basicity ranks as 10%Co-20%Cu/Dol > 10%Ni-20%Cu/Dol > 10%Zn-20%Cu/Dol > 10%Fe-20%Cu/Dol > dolomite.

Consequently, from both CO_2-TPD and NH_3-TPD profiles in Figures 5 and 4, it was observed that all metal modified catalysts as well as dolomite sample exhibited both acid and basic sites but with different amount. Nonetheless, the presence of basic sites in all metal modified catalysts was comparatively lower than its acidity amount. Therefore, it could be suggested that the acid sites of the catalyst dominate and was involve in glycerol hydrogenolysis reaction than its basic site.

SCANNING ELECTRON MICROSCOPY (SEM)

From Figure 6, it was noticed that the individual grains segregation of all samples were tough to be identified. The catalyst particles were in cluster of closely spaced crystals or else aggregated structure with non-rigid shape which thus put emphasis on the macroporous material of the solid catalyst.
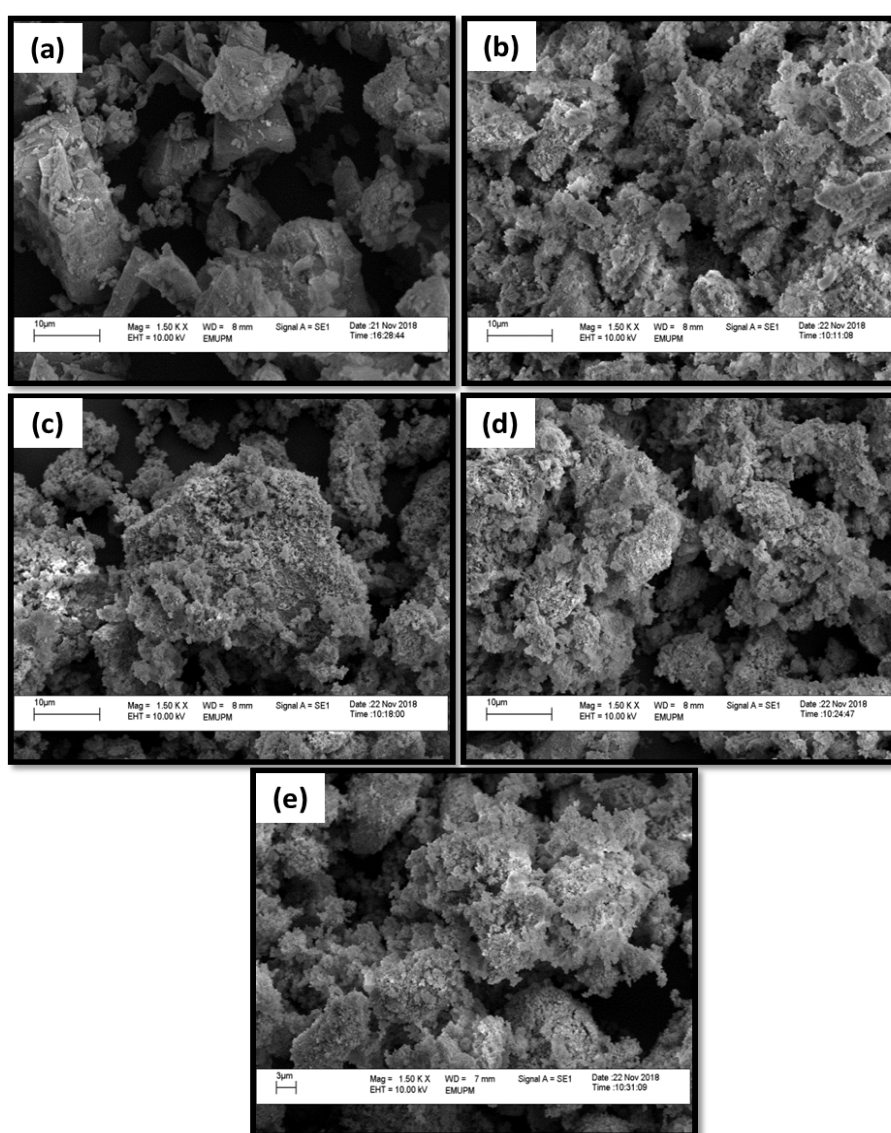

FIGURE 6. SEM images of (a) dolomite, (b) 10%Ni-20%Cu/Dol, (c) 10%Co-20%Cu/Dol, (d) 10%Fe-20%Cu/Dol and (e) 10%Zn-20%Cu/Dol

CATALYTIC ACTIVITY

The experimental results of glycerol hydrogenolysis from Table 2 indicated that the blank reaction was more likely inactive without the presence of any catalyst since the activity was low with only 8.7% GC and none selectivity towards 1,2-PDO was detected.

TABLE 2. Catalytic performance of the synthesised catalysts

Sample	Conversion (%) Acetol	Selectivity (%)			TOF (h^{-1})
		1,2-PDO	Methanol		
Blank	8.7	0	0	0	-
Dolomite	10.6	6.3	0	93.7	0.46
10%Ni-20%Cu/Dol	83.5	20.3	75	4.7	3.63
10%Co-20%Cu/Dol	60.5	21.2	76.5	2.3	2.63
10%Fe-20%Cu/Dol	78.5	13.1	76.1	10.8	3.41
10%Zn-20%Cu/Dol	57.2	25.3	71	3.7	2.48

Reaction conditions: 20 mL of aqueous glycerol (20 wt%); reaction temperature 200 ℃; H$_2$ pressure 4 MPa; catalyst dosage 1 g; reaction time 10 h

As dolomite was involved, a slight increase in glycerol conversion was recorded at 10.6% but still no selectivity to 1,2-PDO. Thus, it was agreed that the support on its own cannot catalyse the hydrogenolysis of glycerol. Nevertheless, for metal modified catalysts, the activity was more significant with 10%Ni-20%Cu/Dol presented the highest glycerol conversion (83.5%) among all the catalysts. In contrast, 10%Co-20%Cu/Dol, 10%Fe-20%Cu/Dol and 10%Zn-20%Cu/Dol catalysts exhibited much lower glycerol conversion of 60.5, 78.5 and 57.2%, respectively. For 1,2-PDO selectivity, the activity of 10%Ni-20%Cu/Dol appeared rather similar with 10%Co-20%Cu/Dol and 10%Fe-20%Cu/Dol in the range 75-76%. Meanwhile, the lowest activity in both GC (57.1%) and 1,2-PDO selectivity (71%) was recorded by 10%Zn-20%Cu/Dol. The catalytic activity ranked as 10%Ni-20%Cu/Dol > 10%Co-20%Cu/Dol ≈ 10%Fe-20%Cu/Dol > 10%Zn-20%Cu/Dol > dolomite.

The higher activity of 10%Ni-20%Cu/Dol catalyst was accredited to its good surface acid sites (adequate acidity) as it is known that during hydrogenolysis reaction, glycerol was formerly adsorbed and then dehydrated on the surface acid sites, and later the dehydrated intermediate (acetol) converted to form final product of 1,2-PDO. Hence, adequate acidity was important to provide a significant amount of acid sites to be accessible for glycerol molecules adsorption. As well, since metallic site was imperative for the hydrogenation of dehydrated intermediate (acetol) to 1,2-PDO, reducibility character of solid catalyst was important. From H$_2$-TPR profile in Figure 3, it was indicated that the reducible oxide species in 10%Ni-20%Cu/Dol catalyst was essentially reduced at the lowest reduction temperature (264 ℃) among the catalysts. Correspondingly, the presence of metallic Cu and Ni species in 10%Ni-20%Cu/Dol catalyst could be associated with its high 1,2-PDO selectivity. Also, as the catalytic reaction was conducted at 200 ℃, therefore, it fitted with the reduction region of metallic copper-nickel species (≥ ~200 ℃).

CONCLUSION

In this present study, several metal modified dolomite catalysts (10%Ni-20%Cu/Dol, 10%Co-20%Cu/Dol, 10%Fe-20%Cu/Dol, and 10%Zn-20%Cu/Dol) were synthesized for glycerol hydrogenolysis and it was found that 10%Ni-20%Cu/Dol catalyst showed with more favorable activity than the other catalysts giving optimum GC and 1,2-PDO selectivity of 83.5% and 75%, respectively at 200 ℃, 4 MPa H$_2$, 10 h duration test, 20 wt% glycerol concentration and 1 g catalyst dosage. The presence of metallic Ni and Cu species, adequate catalyst acidity and good metal reducibility contributed to its catalyst performance. As well, the reduction profile of 10%Ni-20%Cu/Dol occurred within ~ 200 ℃ was adequate for metallic Cu and Ni species stability during catalytic reaction. Furthermore, in this study, a

high catalyst surface area was not the main factor that contributed to the good catalytic activity in all metal modified catalyst than dolomite since the performance was still good with low surface area. Catalyst acidity and metal reducibility could have played dominant role in the reaction performance rather textural property such as types and shape of pores, degrees of porosity, and pore diameter of the catalysts.

ACKNOWLEDGEMENTS

REFERENCES

Asikin-Mijan, N., Lee, H.V., Juan, J.C., Noorsaadah, A.R. & Taufiq-Yap, Y.H. 2017. Catalytic deoxygenation of triglycerides to green diesel over modified CaO-based catalysts. *RSC Advances* 7(73): 46445-46460.

Azri, N., Ramli, I., Nda-Umar, U.I., Shamsuddin, M.R., Saiman, M.I. & Taufiq-Yap. Y.H. 2020. Copper-dolomite as effective catalyst for glycerol hydrogenolysis to 1,2-propanediol. *Journal of the Taiwan Institute of Chemical Engineers* 112: 34-51.

Bagheri, S., Muhd, N. & Yehye, W.A. 2015. Catalytic conversion of biodiesel derived raw glycerol to value added products. *Renewable and Sustainable Energy Reviews* 41: 113-127.

Balaraju, M., Rekha, V., Prasad, P.S.S., Devi, B.L.A.P., Prasad, R.B.N. & Lingaiah, N. 2009. Influence of solid acids as co-catalysts on glycerol hydrogenolysis to propylene glycol over Ru/C catalysts. *Applied Catalysis A: General* 354(1-2): 82-87.

Freitas, I.C., Manfro, R.L. & Souza, M.M.V.M. 2018. Hydrogenolysis of glycerol to propylene glycol in continuous system without hydrogen addition over Cu-Ni catalysts. *Applied Catalysis B: Environmental* 220: 31-41.

Gallegos-Suarez, E., Guerrero-Ruiz, A., Rodriguez-Ramos, I. & Arcoya, A. 2015. Comparative study of the hydrogenolysis of glycerol over Ru-based catalysts supported on activated carbon, graphite, carbon nanotubes and KL-zeolite. *Chemical Engineering Journal* 262: 326-333.

Gandarias, I., Requies, J., Arias, P.L., Armbruster, U. & Martin, A. 2012. Liquid-phase glycerol hydrogenolysis by formic acid over Ni–Cu/Al$_2$O$_3$ catalysts. *Journal of Catalysis* 290: 79-89.

Jiang, T., Kong, D., Xu, K. & Cao, F. 2016. Hydrogenolysis of glycerol aqueous solution to glycols over Ni–Co bimetallic catalyst: Effect of ceria promoting. *Applied Petrochemical Research* 6(2): 135-144.

Karelovic, A. & Ruiz, P. 2015. The role of copper particle size in low pressure methanol synthesis via CO$_2$ hydrogenation over Cu/ZnO catalysts. *Catalysis Science & Technology* 5(2): 869-881.

Kovanda, F., Jiratova, K., Rymes, J. & Kolousek, D. 2001. Characterization of activated Cu/Mg/Al hydrotalcites and their catalytic activity in toluene combustion. *Applied Clay Science* 18(1-2): 71-80.

Li, Y., Guo, Y. & Xue, B. 2009. Catalytic combustion of methane over M (Ni, Co, Cu) supported on ceria-magnesia. *Fuel Processing Technology* 90(5): 652-656.

Luna, F.M.T., Cecilia, J.A., Saboya, R.M.A., Barrera, D., Sapag, K., Rodríguez-Castellón, E. & Calvancante Jr., C.L. 2018. Natural and modified montmorillonite clays as catalysts for synthesis of biolubricants. *Materials* 11(9): 1764.

Mallesham, B., Sudarsanam, P., Reddy, B.V.S. & Reddy, B.M. 2016. Development of cerium promoted copper – magnesium catalysts for biomass valorization: Selective hydrogenolysis of bioglycerol. *Applied Catalysis B: Environmental* 181: 47-57.

Nagaraja, B.M.P., Seetharamulu, A.H., Reddy, P.K.H.P., Raju, B.D. & Rao, K.S.R. 2007. A highly active Cu-MgO-Cr$_2$O$_3$ catalyst for simultaneous synthesis of furfuryl alcohol and cyclohexanone by a novel coupling route - combination of furfural hydrogenation and cyclohexanol dehydrogenation. *Journal of Molecular Catalysis A: Chemical* 278(1-2): 29-37.

Pandhare, N.N., Pudi, S.M., Biswas, P. & Sinha, S. 2016. Vapor phase hydrogenolysis of glycerol to 1, 2-propanediol over γ-Al$_2$O$_3$ supported copper or nickel monometallic and copper-nickel bimetallic catalysts. *Journal of the Taiwan Institute of Chemical Engineers* 61: 90-96.

Pardeshi, S.K. & Pawar, R.Y. 2010. Optimization of reaction conditions in selective oxidation of styrene over fine crystallite spinel-type CaFe$_2$O$_4$ complex oxide catalyst. *Materials Research Bulletin* 45(5): 609-615.

Priya, S.S., Selvakannan, P.R., Chary, K.V.R., Kantam, M.L. & Bhargava, S.K. 2017. Solvent-free microwave-assisted synthesis of solketal from glycerol using transition metal ions promoted mordenite solid acid catalysts. *Molecular Catalysis* 434: 184-193.

Pudi, S.M., Biswa, P., Kumar, S. & Sarkar, B. 2015. Selective hydrogenolysis of glycerol to 1,2 propanediol over bimetallic Cu-Ni catalysts supported on γ-Al$_2$O$_3$. *Journal of the Brazilian Chemical Society* 268(8): 1551-1564.

Putrakumar, B., Nagaraju, N., Kumar, V.P. & Chary, K.V.R. 2015. Hydrogenation of levulinic acid to valerolactone over copper catalysts supported on Al$_2$O$_3$. *Catalysis Today* 250: 209-217.

Rahman, N., Ramli, A., Jumbri, K. & Uemura, Y. 2019. Tailoring the surface area and the acid-base properties of ZrO$_2$ for biodiesel production from *Nannochloropsis* sp. *Scientific Reports* 9: 16223.

Rajkhowa, T., Marin, G.B. & Thybaut, J.W. 2017. A comprehensive kinetic model for Cu catalyzed liquid phase glycerol hydrogenolysis. *Applied Catalysis B: Environmental* 205: 469-480.

Soares, A.V.H., Perez, G. & Passos, F.B. 2016a. Alumina supported bimetallic Pt–Fe catalysts applied to glycerol hydrogenolysis and aqueous phase reforming. *Applied Catalysis B: Environmental* 185: 77-87.

Soares, A.V.H., Salazar, J.B., Falcone, D.D., Vasconcellos, F.A., Davis, R.J. & Passos, F.B.A. 2016b. Study of glycerol hydrogenolysis over Ru–Cu/Al$_2$O$_3$ and Ru–Cu/ZrO$_2$ catalysts. *Journal of Molecular Catalysis A: Chemical* 415: 27-36.

Srivastava, S., Jadeja, G.C. & Parikh, J. 2017. Synergism studies on alumina-supported copper nickel catalysts towards furfural and 5-hydroxymethylfurfural hydrogenation. *Journal of Molecular Catalysis A: Chemical* 426: 244-256.

Tanasoi, S., Tanchoux, N., Adriana, U., Tichit, D., Sandulescu, I., Fajula, F. & Marcu, I.C. 2009. New Cu-based mixed oxides obtained from LDH precursors, catalysts for methane total oxidation. *Applied Catalysis A: General* 363(1-2): 135-142.

Tasyurek, K.C., Bugdayci, M. & Yucel, O. 2018. Reduction conditions of metallic calcium from magnesium production residues. *Metals* 8(383): 1-14.

Thirupathi, B. & Smirniotis, P.G. 2012. Nickel-doped Mn/TiO$_2$ as an efficient catalyst for the low-temperature SCR of NO with NH$_3$: Catalytic evaluation and characterizations. *Journal of Catalysis* 288: 74-83.

Vargas-Hernández, D., Rubio-Caballero, J.M., Santamaría-González, J., Moreno-Tost, R., Mérida Robles, J.M., Pérez-Cruz, M.A., Jiménez-López, A., Hernández-Huesca, R. & Maireles-Torres, P. 2014. Furfuryl alcohol from furfural hydrogenation over copper supported on SBA-15 silica catalysts. *Journal of Molecular Catalysis A: Chemical* 383-384: 106-113.

Vasiliadou, E.S. & Lemonidou, A.A. 2011. Investigating the performance and deactivation behaviour of silica-supported copper catalysts in glycerol hydrogenolysis. *Applied Catalysis A: General* 396(1-2): 177-185.

Wen, C., Yin, A., Cui, Y., Yang, X., Dai, W.L. & Fan, K. 2013. Enhanced catalytic performance for SiO$_2$-TiO$_2$ binary oxide supported Cu-based catalyst in the hydrogenation of dimethyloxalate. *Applied Catalysis A: General* 458: 82-89.

Xia, S., Yuan, Z., Wang, L., Chen, P. & Hou, Z. 2011. Hydrogenolysis of glycerol on bimetallic Pd-Cu/solid-base catalysts prepared via layered double hydroxides precursors. *Applied Catalysis A: General* 403: 173-182.

Yu, W., Zhao, J., Ma, H., Miao, H., Song, Q. & Xu, J. 2010. Aqueous hydrogenolysis of glycerol over Ni-Ce/AC catalyst: Promoting effect of Ce on catalytic performance. *Applied Catalysis A: General* 383: 73-78.

Zhao, F., Li, S., Wu, X., Yue, R., Li, W., Zha, X., Deng, Y. & Chen, Y. 2019. Catalytic behaviour of flame-made CuO-CeO$_2$ nanocatalysts in efficient Co oxidation. *Catalyst* 9(3): 256.

Zhao, S., Yue, H., Zhao, Y., Wang, B., Geng, Y., Jing, Lv., Wang, S., Gong, J. & Ma, X. 2013. Chemoselective synthesis of ethanol via hydrogenation of dimethyl oxalate on Cu/SiO$_2$: Enhanced stability with boron dopant. *Journal of Catalysis* 297: 142-150.

Zheng, L., Xia, S. & Hou, Z. 2015. Hydrogenolysis of glycerol over Cu-substituted hydrocalumite mediated catalysts. *Applied Clay Science* 118: 68-73.

Zhu, S., Gao, X., Zhu, Y., Zheng, H. & Li, Y. 2013. Promoting effect of boron oxide on Cu/SiO$_2$ catalyst for glycerol hydrogenolysis to 1,2-propanediol. *Journal of Catalysis* 303: 70-79.

*Corresponding author; email: irmawati@upm.edu.my